

## Purdue University Purdue e-Pubs

---

International Compressor Engineering Conference

School of Mechanical Engineering

---

1998

# Development of the Materials for Sliding Parts of the Compressor for HFC's

Y. Futagami

*Matsushita Electric Industrial Co.*

H. Hirano

*Matsushita Electric Industrial Co.*

M. Esumi

*Matsushita Electric Industrial Co.*

H. Oka

*Matsushita Electric Industrial Co.*

H. Kawano

*Matsushita Electric Industrial Co.*

*See next page for additional authors*

Follow this and additional works at: <https://docs.lib.purdue.edu/icec>

---

Futagami, Y.; Hirano, H.; Esumi, M.; Oka, H.; Kawano, H.; and Nakajima, K., "Development of the Materials for Sliding Parts of the Compressor for HFC's" (1998). *International Compressor Engineering Conference*. Paper 1229.  
<https://docs.lib.purdue.edu/icec/1229>

This document has been made available through Purdue e-Pubs, a service of the Purdue University Libraries. Please contact [epubs@purdue.edu](mailto:epubs@purdue.edu) for additional information.

Complete proceedings may be acquired in print and on CD-ROM directly from the Ray W. Herrick Laboratories at <https://engineering.purdue.edu/Herrick/Events/orderlit.html>

---

**Authors**

Y. Futagami, H. Hirano, M. Esumi, H. Oka, H. Kawano, and K. Nakajima

# Development of the materials for sliding parts of the compressor for HFC's

Yoshiyuki Futagami<sup>1</sup>, Hideo Hirano<sup>2</sup>, Mototaka Esumi<sup>3</sup>  
Hideto Oka<sup>3</sup>, Hiroyuki Kawano<sup>4</sup>, Keizo Nakajima<sup>5</sup>

<sup>1</sup>Engineer, Air Conditioning Research Laboratory,

<sup>2</sup>Senior Staff Engineer, Air Conditioning Research Laboratory,

<sup>3</sup>Senior Engineer, Compressor Division,

<sup>4</sup>Engineer, Compressor Division,

Matsushita Electric Industrial Co., Ltd. (Panasonic),

Nojihigashi, Kusatsu-shi, Shiga 525-8520, Japan.

Tel:81-77-567-9801, Fax:81-77-561-3201

E-mail: PAN23941@pas.mei.co.jp

<sup>5</sup>Senior Researcher, Human Environmental Systems Development Center

Yagumo-nakamachi, Moriguchi, Osaka 570-8501, Japan.

## Abstract

To improve the severe sliding conditions, that is caused by the combination of HFC's and ester-oil, we conducted the following steps. First, We studied the wear-mechanism in ester-oil, and got the following results

1. The wear has close relation with chemical reaction.
2. The temperature of the sliding part will affect greatly the reaction.

Second, to improve the durability of materials for the corrosive-wear, We focused on the followings.

1. Maintaining the thickness of oil-film.
2. Improving the anti-corrosion property.

Finally, We developed new materials with high wear resistant property, and achieved the great improvement of the reliability of the compressor for HFC's.

## 1.Introduction

In January 1998, our company released room air-conditioners utilizing HFC refrigerant (R410A) which does not deplete the ozone layer. The lubrication oil used for this compressor is VG68 ester oil which is highly soluble in R410A. Ester oil has lower lubricating performance than that of conventional mineral oil in R22. Ester oil, when mixed with water, causes hydrolysis and a unique wear phenomenon called corrosive-wear. Iron soap, the reactive product of corrosive-wear, clogs capillary tubes. If water content is minimized to limit hydrolysis, the reaction shifts to corrosive-wear caused by thermal decomposition, interfering with good lubrication. The problem with commercial use of ester oil was identified as the need to control corrosive-wear induced by thermal decomposition. To limit thermal decomposition, efforts were made to increase the thermal stability of ester oil through studies of the chemical structure of the base oil and the use of additives.<sup>1)</sup> The oil film retaining capability and corrosion resistant properties of the sliding components were also improved to obtain the same or better wear resistance as that for mineral oil in R22. This paper reports the conditions under which corrosive-wear is caused by ester oil and on the sliding materials best suited to the ester oil.

## 2. Ester Oil Specifications

Ester oil is synthesized from fatty acids and an alcohol. A study was carried out on the relationship between the chemical structure of the fatty acid and its thermal stability. Although the lubrication performance of ester oils with linear fatty acids is known to be superior to that of ester oils with branched fatty acids, a sealed tube test and wear test were carried out first. Results showed that the ester oil with the branched fatty acids was found to be superior to the ester oil with linear fatty acids in thermal stability. In particular, the branched fatty acid iC8 which has a branch at the alpha position is superior in thermal stability and effectiveness in suppressing iron soap generation in addition to superior lubrication performance.

Next, an accelerated test of a rotary compressor was carried out. The results are shown in Fig. 1. It was confirmed that the ester oil with branched fatty acids was superior in lubrication performance to ester oil with linear fatty acids, since it demonstrated less wear on the vane and piston. In an attempt to obtain transient characteristics comparable to those of conventional oil, an ester oil containing a mixture ratio of fatty acid iC8/ iC9=50/50 and pentaerythritol was selected. The final specification was made by adding acid absorbers to improve thermal stability and further adding anti-oxidants to suppress reactions caused by oxygen dissolved in the oil.

### 3. Conditions Causing Corrosive-wear

#### 3.1 Evaluation of Static Thermal Stability of the Ester Oil

A sealed tube test was conducted on the ester oil. A piece of iron 1.2 mm in diameter and 50 mm in length and copper and aluminium pieces each 1.0 mm diameter and 50 mm in length were sealed in a glass tube evacuated to a pressure of  $5 \times 10^{-4}$  torr. After applying heat for 120 hours in a convention oven, the generated gas was analyzed using gas chromatography.

The temperature characteristics of the volume of generated gas are shown in Fig. 2. Generation of non-condensing gases such as CO, CO<sub>2</sub>, and H<sub>2</sub> can be observed. At the same time, an increase of iron ion concentration can be seen, indicating thermal decomposition of ester oil accompanied by generation of iron soap. It is assumed that the focus of decomposition was mainly near the carbonyl group, resulting in the generation of CO and CO<sub>2</sub>. Although differential scanning calorimetry indicates that the thermal decomposition temperature of this compound mix in nitrogen gas exceeds 400 °C, the measured thermal decomposition temperature was significantly lower at 250 °C due to the existence of iron. Knowing that the temperature of the non-sliding parts of a compressor is much lower than 250°C, it is clear that thermal decomposition of the ester oil does not occur at these locations.

#### 3.2 Evaluation of Dynamic Thermal Stability of the Ester Oil

To evaluate the thermal stability of ester oil with the activated iron, pure iron pieces were tumbled to peel off the oxidized surface in the ester oil. The experimental equipment is shown in Fig. 3. It is a 300 ml three-pronged flask with a stirrer, argon gas inlet and gas outlet attached to it. Ester oil and pure iron pieces 10 x 4 x 4 mm in size were placed inside the three-pronged flask and the flask was kept at a fixed temperature using a heated bath. The oil and iron particles were stirred while introducing argon gas, and the generated gas was analyzed using gas chromatography.

The relation between temperature and volume of generated hydrogen gas after two hours are shown in Fig. 4. The volume of generated hydrogen gas increases sharply at 200 °C and the thermal decomposition temperature of the ester

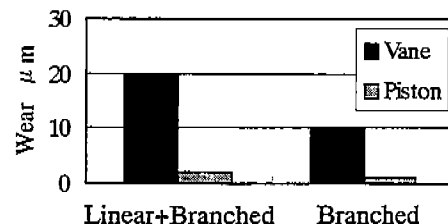


Fig.1 Accelerated test of a rotary compressor

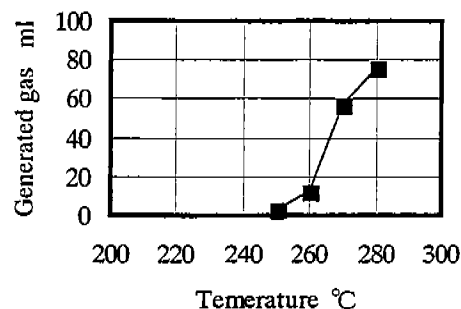


Fig.2 Static thermal stability

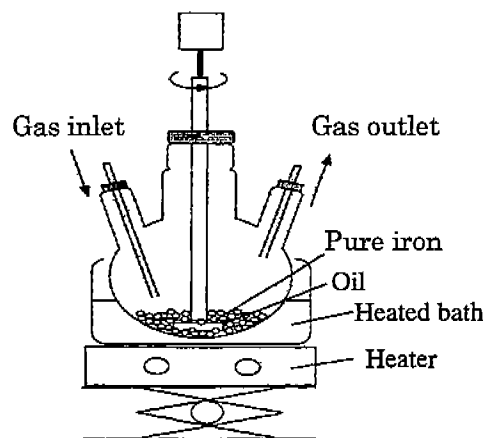


Fig.3 Experimental equipment

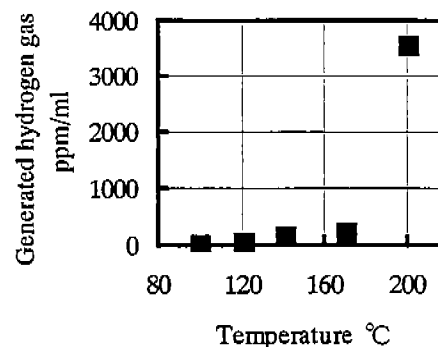


Fig.4 Dynamic thermal stability

oil falls to below the result demonstrated in the static thermal stability evaluation. These results indicate that thermal decomposition of ester oil is caused at a relatively low temperature on an iron surface which is activated by friction between pure iron particles. This means that the temperature at sliding parts under boundary lubrication or mixed lubrication conditions is a key factor in the behavior of ester oil.

### 3.3 Surface Temperature on Sliding Parts

A new attempt to measure the surface temperature of sliding parts using a wear tester is described.

Special attention was paid to the slide between the vane and piston of a rotary compressor, the area that is believed to experience the most severe lubrication conditions within the compressor of a room air- conditioner. The sliding conditions in an accelerated test were modeled : the wear test conditions shown in Table 1 were reproduced using the high-pressure atmosphere wear tester illustrated in Fig. 5. The shape of the tested vane is shown in Fig. 6. The initial surface roughness of the vane and disk was Ra 0.08. The tip of the vane had an equivalent radius.

Carbon tool steel (SK5) was selected for the vane. The surface temperature at the tip of the vane was measured by utilizing the tempering temperature characteristics of Hv hardness shown in Fig. 7. The disk material used for the test was special alloy cast iron. The SK5 material was hardened at 780 °C and tempered at 100 °C for 2 hours. The Vickers hardness was measured on the sliding surface at the tip of the vane after the wear test and was converted to the corresponding temperature to obtain the surface temperature. The hardness distribution in the depth direction is shown in Fig. 8, and the temperature distribution of the sliding surface is shown in Fig. 9. A large decrease in hardness may be noticed in the range 20  $\mu$ m from the surface, indicating a large thermal gradient. The surface temperature at the tip of the vane was 201 to 323 °C, relatively high compared to the oil temperature, and well within the range in which thermal decomposition takes place.

An accelerated test of a room air conditioner with a rotary compressor was carried out using an iron alloy vane. The results showed an increase in iron ion concentration in the oil and capillary clogging by accumulated iron soap, proving that the surface temperature at the tip of the vane was exceeding

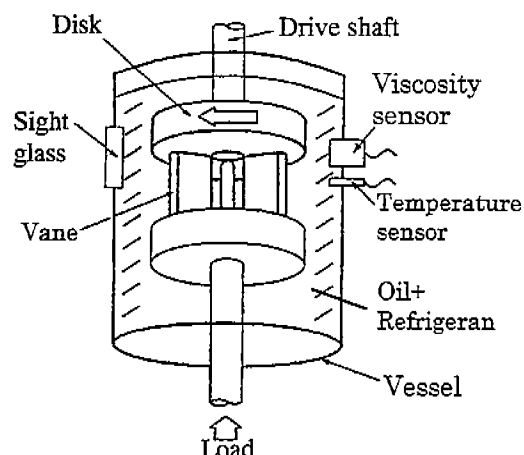


Fig.5 Wear tester

Table 1 Test conditions

Refrigerant	R134a
Oil Temperature	383 K
Vessel Pressure	1.42 MPa
Load	1.47 KN
Speed	500 min <sup>-1</sup>
Time	3 h

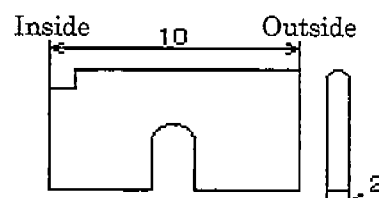


Fig.6 Vane

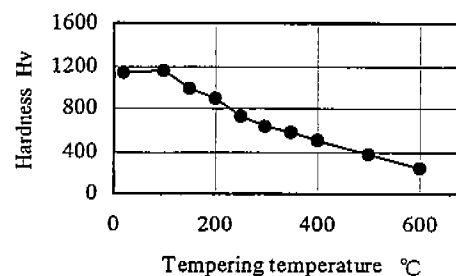


Fig.7 Hardness vs. tempering temperature

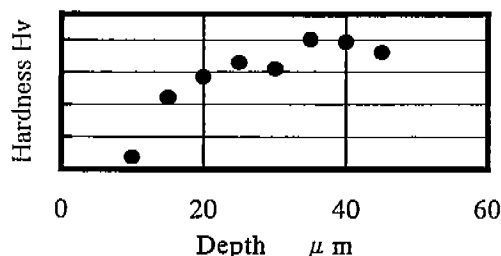


Fig.8 Hardness distribution in the depth direction

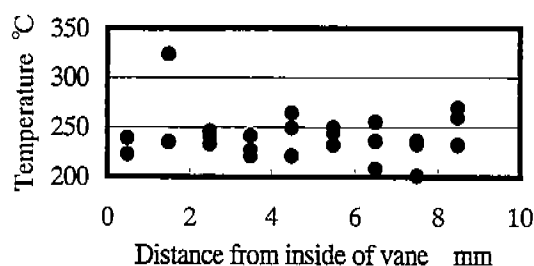


Fig.9 Temperature distribution of the sliding surface

200 °C in some areas during actual operation. This meant that countermeasures were required for iron-based sliding parts, such as the vane tip, which are exposed to high temperatures.

#### 4. Changes to Sliding Materials to Match the Characteristics of the Ester Oil

The structure of a small horizontal type scroll compressor is shown in Fig. 10. The compressing mechanism consists of a fixed scroll and a orbiting scroll which engages with the fixed scroll and traces a orbiting motion. The fixed scroll is made from cast iron, and the orbiting scroll is made from aluminium alloy to make it low-mass and thus able to withstand high rotation speeds. The orbiting scroll has a part which is driven via the center of the end plate by the function of an eccentric bearing on the main shaft and an Oldham ring located behind the end plate of the orbiting scroll. The eccentric bearing and the Oldham ring are made from sintered iron.

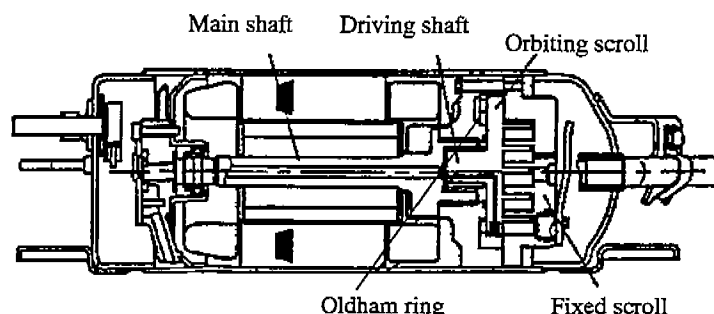


Fig.10 Configuration of horizontal-type scroll compressor

The sliding parts of this scroll compressor, the eccentric bearing which often tends to reach a high temperature, and the Oldham ring operating under mixed lubrication conditions were studied for their suitability for use with the ester oil. Corrosive-wear was suppressed by controlling the activation of the iron surface using the followings.

- (1) The oil film retaining capability of the eccentric bearing was strengthened.
- (2) The anti-corrosion property for the Oldham ring was improved.

##### 4.1 Strengthening Oil Film Retaining Capability

The relationship between the pore specification of sintered iron and oil film retaining capability was examined. The load characteristics of coefficient of friction obtained from a wear test are shown in Fig. 11. The oil film retaining capability was measured at the load at which coefficient of friction sharply increased, and the load at which coefficient of friction exceeded 0.20 was designated as the seizure load. The partner material was aluminium alloy.

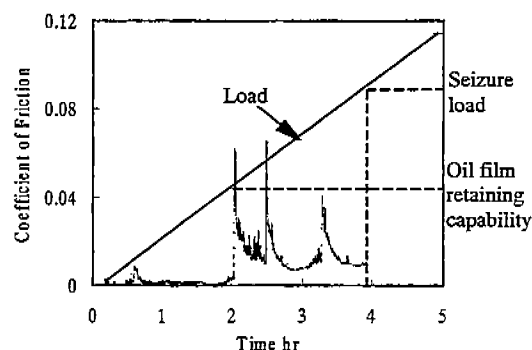


Fig.11 Load characteristic of coefficient of friction

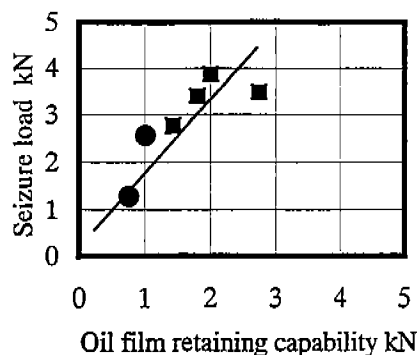


Fig.12 Seizure load vs. oil retaining capability

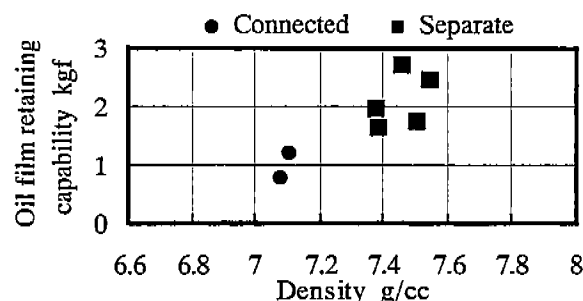


Fig.13 Oil retaining capability vs. Density

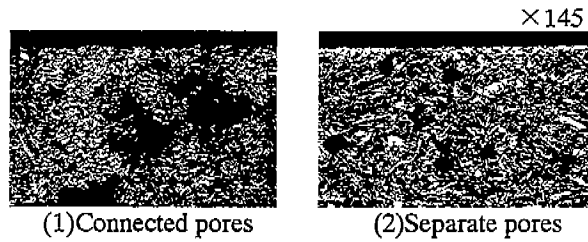


Fig.14 Sectional structure

capability and material density is shown in Fig. 13. The oil film retaining capability improves with material density. The sectional structure of a surface layer of a sliding surface is shown in Fig. 14. Connected pores are visible in the low density material while separate pores are evident in the higher density material. It can be assumed that the oil-filled separate pores improve the oil film retaining capability.

Because variations in oil film retaining capability were noticeable even using the same density material with separate pores, the difference in pore distribution was examined. The sintered irons after testing were ground and buffed, and the pore distribution on the sliding surface was observed using a scanning laser microscope. Images from an area of 1235 x 941  $\mu\text{m}$  viewed by the scanning laser microscope were taken for binarization and a binary image was made as shown in Fig. 15. The pore distribution condition was examined by analyzing the binary image. Shown in Fig. 16 is the relationship between the oil retaining capability and the area ratio, which is the ratio of area occupied by pores compared with the entire area. For separate pores, oil film retaining capability increases with a reduction of area ratio. On the other hand, the oil film retaining capability does not increase with a reduction of area ratio for connected pores. The relationship between equivalent circle diameters and their frequency is shown in Fig. 17. The relationship between the ratio of pores 10  $\mu\text{m}$  or smaller from Fig. 17 and the oil film retaining capability is shown in Fig. 18. It is evident that the oil film retaining capability rises to more than double that of a material with connected pores when the ratio of pores of size 10  $\mu\text{m}$  or smaller is 90.3% or higher.

Based on the above examinations, the oil film retaining capability of sintered iron material can be improved by up to more than two times by optimizing the pore distribution to improve the durability in a high load range.

#### 4.2 Improving Anti-corrosion Properties

On the sliding surfaces in a mixed lubrication region, corrosive-wear is caused by thermal decomposition of ester oil on the high temperature activated iron surface. This means that a highly corrosion resistant material would be chemically stable and effective in suppressing corrosive-wear.

The relationship between the surface treatment and corrosion resistance of sintered iron was examined. Shown in Fig. 19 is the result of a wear test using gray cast iron (FC250).

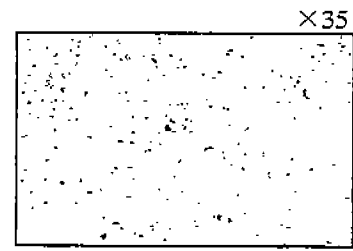


Fig.15 Binary image

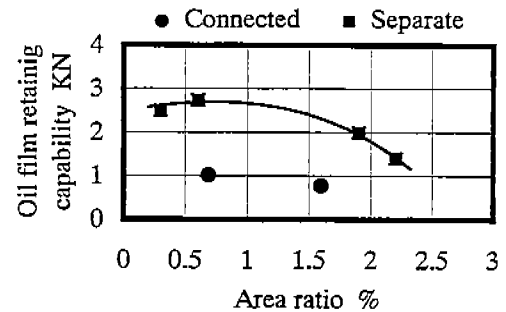


Fig.16 Oil retaining capability vs. area ratio

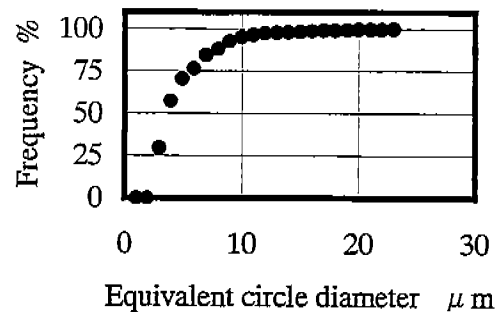


Fig.17 Distribution of pore diameter

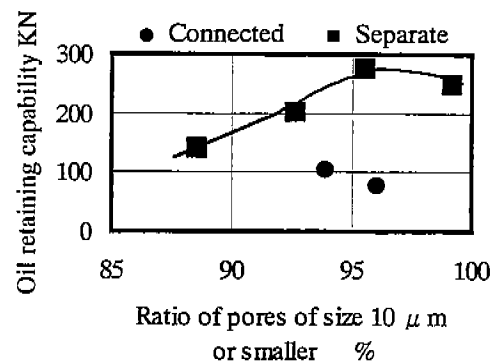


Fig.18 Oil retaining capability vs. distribution of pore diameter

When sintered iron is treated by steam treatment and gas nitrocarburizing, the amount of wear and iron ion concentration in the oil of it are smaller than those of sintered iron without surface treatment. This is the result of the suppression of corrosive-wear by a chemically stable and corrosion resistant oxide or nitriding layer formed on the surface.

The result of a wear test on aluminium alloy is shown in Fig. 20. It shows that the gas nitrocarburizing is superior in wear resistance but the steam treatment has greater partner-biting properties. Shown in Fig. 21 is the sectional structure of its surface layer and shown in Fig. 22 is the load characteristics of coefficient of friction. The material treated with gas nitrocarburizing ensures that the oil film retaining capability has low partner-biting properties. On the other hand, the material treated with oxidation is low in oil film retaining capability and attacks low hardness aluminium alloy.

A scroll compressor, with its eccentric bearing made from sintered iron with the optimized pore specification, and an Oldham ring made also from sintered iron with its sliding surface treated with gas nitrocarburizing, was installed in a room air conditioner for an accelerated test. Results confirmed that the reliability was at the same level or higher than that of conventional mineral oil in R22.

## 5. Conclusions

The results of an examination of the conditions under which ester oil causes corrosive-wear, and the slide materials best suited for use with ester oil, indicate the followings.

1. Ester oil is subject to thermal decomposition at approximately 200 °C on surfaces activated by friction with iron.
2. Selection of material for sliding parts is important for matching the ester oil at the high temperature sliding surface under mixed lubrication conditions.
3. A material with high oil film retaining capability or high anti-corrosion property is best suited for sliding parts.
4. Good affinity of sintered iron to ester oil has been achieved by strengthening the oil film retaining capability with optimized pore distribution or improving the anti-corrosion property by gas nitrocarburizing.

## 6. References

- 1) S. Hase et al., "Development of a Compact Horizontal-Type Scroll Compressor for Alternative Refrigerants", Proc. International Compressor Engineering Conference at Purdue, Vol.1, 1996, pp.303-309

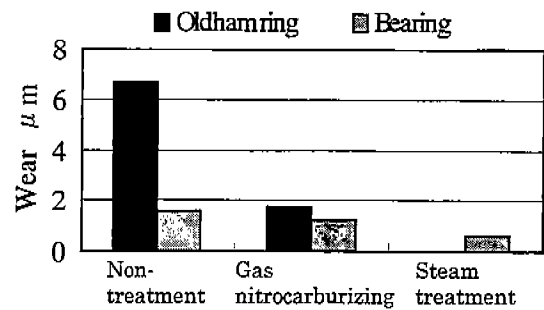


Fig.19 Wear test result (FC250)

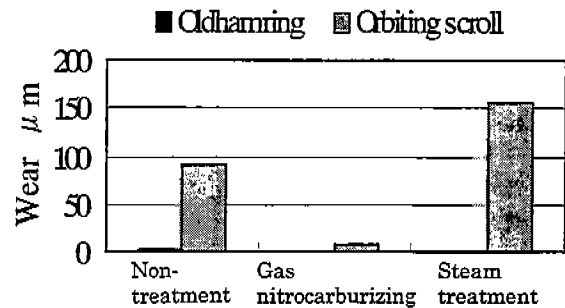


Fig.20 Wear test result (aluminum alloy)

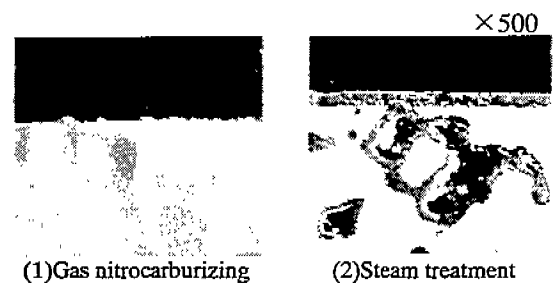


Fig.21 Sectional structure of surface layer

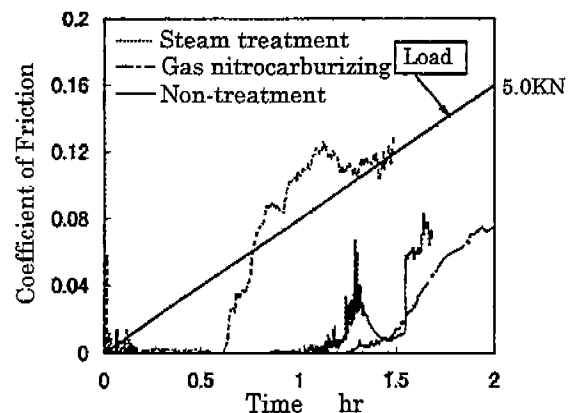


Fig.22 Load characteristics of coefficient of friction